Implementation of new diffusion/filtering operators in the CAM-FV dynamical core

Peter H. Lauritzen[a,*], Arthur A. Mirin[b], John Truesdale[a], Kevin Raeder[c], Jeffrey L. Anderson[c], Julio Bacmeister[a], Richard B. Neale[a]

[a]*Climate and Global Dynamics Division, National Center for Atmospheric Research, 1850 Table Mesa Drive, Boulder, CO 80305, Boulder, USA*
[b]*Lawrence Livermore National Laboratory, Box 808, L-561 Livermore, CA 94551-0808, USA*
[c]*Institute for Mathematics Applied to Geosciences, National Center for Atmospheric Research, 1850 Table Mesa Drive, Boulder, CO 80305, USA*

Abstract

Two new filtering/diffusion operators have been implemented in the Community Atmosphere Model finite-volume dynamical core (CAM-FV). First, a fourth-order divergence damping operator has been added to optionally replace the second-order version that has traditionally been used. This provides more scale selective dissipation of divergent modes that can generate grid-scale noise in CAM-FV if not damped properly. For example, data-assimilation runs using CAM-FV DART (Data Assimilation Research Testbed) have revealed potential noise problems at the grid scale that can be alleviated significantly using higher-order divergence damping. Second, a 'Laplacian'-type damping operator has been implemented to increase the explicit momentum dissipation in the top-of-atmosphere sponge layers. This helps control the excessive polar night jets that have been observed in ultra-high resolution CAM-FV simulations. Results from stand-alone CAM-FV and CAM-FV DART are presented in this paper along with details on the implementation of the new operators.

Keywords: Divergence damping, Laplacian damping, High-resolution climate simulation, Data-assimilation, Finite-volume

1. Introduction

Most numerical weather prediction and climate models need diffusion/filtering operators throughout the domain in order to be 'well-behaved' for the smallest scales represented. In addition, enhanced diffusion/filtering is usually required in sponge layers near model boundaries to avoid numerical problems like the spurious reflection of vertically propagating waves. Unfortunately, the use and implementation of diffusion and filtering operators is rarely documented, discussed and analyzed in the literature. A notable exception is the recent book chapter

*Corresponding author. Tel.: +1 303 497 1316; fax: +1 303 497 1324.
Email address: pel@ucar.edu (Peter H. Lauritzen)
URL: http://www.cgd.ucar.edu/cms/pel/ (Peter H. Lauritzen)
[1]The National Center for Atmospheric Research is sponsored by the National Science Foundation.

by Jablonowski and Williamson (2010). Numerical noise and instabilities in weather and climate models can lead to model failure and contaminate results.

The purpose of this paper is to document and assess new damping/filtering operators in NCAR's Community Atmosphere Model Finite-Volume version (CAM-FV; Lin 2004, Neale et al. 2010a). These enhance the model's functionality and capability. In particular, the new damping/filtering operators increase the model's robustness at high horizontal resolution, alleviate the excessive polar night jet that develops in 'default' high resolution CAM-FV simulations and reduce grid-scale noise. The need to filter grid-scale noise is also increased when CAM-FV is used with DART (Data Assimilation Research Testbed; Anderson et al. 2009) for data assimilation.

The paper is organized as follows. In section 2 the continuous form of the divergence and 'Laplacian'-type damping operators are presented followed by their discretization on the regular latitude-longitude grid used by CAM-FV. In section 3 the effect of the new damping/filtering operators in CAM-FV simulations are discussed. This includes their effect on the total kinetic energy (TKE) spectra, the level of noise in the divergence field, the impact in CAM-FV DART setup and their effect on climate. Conclusions are given in section 4.

2. Implementation

2.1. Divergence damping in the continuous momentum equations

The momentum equations in CAM-FV, without explicit diffusion operators, are written in 'vector invariant' form

$$\frac{\partial u}{\partial t} = \Omega v - \frac{1}{a\cos\theta}\Big(\frac{1}{\rho}\frac{\partial p}{\partial \lambda} + \frac{\partial}{\partial \lambda}\left[\mathcal{K} + \Phi\right]\Big) \tag{1}$$

$$\frac{\partial v}{\partial t} = -\Omega u - \frac{1}{a}\Big(\frac{1}{\rho}\frac{\partial p}{\partial \theta} + \frac{\partial}{\partial \theta}\left[\mathcal{K} + \Phi\right]\Big), \tag{2}$$

(Lin, 2004). In the equations above u and v are the zonal and meridional components of the velocity vector $\vec{v} = (u, v)$ in 'shallow atmosphere' spherical coordinates (a,λ,θ), where a is constant (radius of the Earth), $\lambda \in [0, 2\pi]$ is longitude and $\theta \in [-\pi/2, \pi/2]$ latitude. The horizontal kinetic energy is given by $\mathcal{K} = \frac{1}{2}\left(u^2 + v^2\right)$, and Ω, ρ, p, Φ and t are the absolute vorticity, density, pressure, geopotential, and time, respectively.

The discretization of (1) and (2) used in CAM-FV is designed to damp vorticity at the grid scale by using the so-called '**CD**'-grid discretization approach (Lin and Rood, 1997) and through the application of shape-preserving constraints in the transport operator (Lin and Rood, 1996) [2]. However, this formulation does not control divergent modes near the grid scale. To avoid spurious accumulation of the divergent component of TKE near the grid scale, explicit diffusion operators are therefore necessary in CAM-FV. Since the rotational modes are already sufficiently damped near the grid-scale by inherent numerical diffusion (limiters in the transport operator), it is only necessary to explicitly damp the divergent modes. Explicit diffusion that only damps divergent and not rotational modes is referred to as 'divergence damping' (Haltiner and Williams, 1980). Divergence damping is used to control/damp noise in weather and climate models and to enhance numerical stability (e.g. Bates et al., 1993).

[2] for a linear stability analysis of the Lin and Rood (1996) scheme and **CD**-grid discretization technique see Lauritzen (2007) and Skamarock (2008), respectively.

Divergence damping of order n ($n = 2, 4, ...$) is introduced in CAM-FV by adding divergence damping terms on the right-hand side of the momentum equations (1) and (2)

$$\frac{\partial u}{\partial t} = \cdots + \frac{1}{a\cos\theta}\frac{\partial}{\partial\lambda}(\gamma_n\nabla^{n-2}D) \tag{3}$$

$$\frac{\partial v}{\partial t} = \cdots + \frac{1}{a}\frac{\partial}{\partial\theta}(\gamma_n\nabla^{n-2}D). \tag{4}$$

where γ_n is the damping coefficient. The divergence D and Laplacian ∇^2-operator, for a generic scalar ψ, are given by

$$D = \nabla\cdot\vec{v} = \frac{1}{a\cos\theta}\left[\frac{\partial u}{\partial\lambda} + \frac{\partial(v\cos\theta)}{\partial\theta}\right], \tag{5}$$

$$\nabla^2\psi = \frac{1}{a^2\cos^2\theta}\frac{\partial^2\psi}{\partial^2\lambda} + \frac{1}{a^2\cos\theta}\frac{\partial}{\partial\theta}\left(\cos\theta\frac{\partial\psi}{\partial\theta}\right), \tag{6}$$

respectively. In the original formulation of CAM-FV second-order ($n = 2$) divergence damping was used. A purpose of this paper is to document the implementation of fourth-order ($n = 4$) divergence damping which is an option in CAM5 (Neale et al., 2010a).

That the explicit diffusion terms in (3) and (4) damp divergent modes can easily be shown by applying the divergence operator to $\partial\vec{v}/\partial t$ and substituting (3) and (4)

$$\frac{\partial D}{\partial t} = \frac{\partial}{\partial t}\nabla\cdot\vec{v} = \cdots + \nabla^n\left(\gamma_n D\right). \tag{7}$$

Similarly, by applying the curl-operator instead of the divergence operator the damping terms 'drop out'

$$\frac{\partial\eta}{\partial t} = \cdots + \nabla\times\nabla^{n-2}\left(\gamma_n\nabla\cdot\vec{v}\right) = \cdots + 0. \tag{8}$$

Hence vorticity, $\eta = \nabla\times\vec{v}$, is not affected by the divergence damping (at least not in the continuous case).

2.2. Discretization of divergence damping operators

The horizontal staggering of the prognostic variables in CAM-FV is an Arakawa **D** grid (see Figure 1). This allows for a compact centered finite-difference approximation to divergence at the control volume edges (corners; filled circles in Fig. 1)

$$D_{ij} = \frac{1}{a\cos\theta_j}\left[\frac{u_{ij} - u_{i-1\,j}}{\Delta\lambda} + \frac{v_{ij}\cos\theta_j - v_{ij-1}\cos\theta_{j-1}}{\Delta\theta}\right], \tag{9}$$

where (i, j) are the horizontal indices, θ_j is the latitude of cell (i, j)-th center (computed consistently with the finite-volume approach) and $\theta_{j-1/2}$ is the latitude at the south cell edge (for notational clarity the vertical index k has been left out). The grid spacing in longitude and latitude is denoted $\Delta\lambda$ and $\Delta\theta$, respectively.

For the fourth-order divergence damping ($n = 4$) the Laplacian of D_{ij} must be computed. For that, centered finite-differences can conveniently be used

$$\left(\nabla^2 D\right)_{ij} = \frac{1}{a^2\cos^2\theta_j}\frac{D_{i+1\,j} - 2D_{ij} + D_{i-1\,j}}{(\Delta\lambda)^2} + \frac{1}{a^2\cos\theta_j}\frac{(\cos\theta_j)\left(D_{ij+1} - D_{ij}\right) - (\cos\theta_{j-1/2})\left(D_{ij} - D_{ij-1}\right)}{(\Delta\theta)^2}. \tag{10}$$

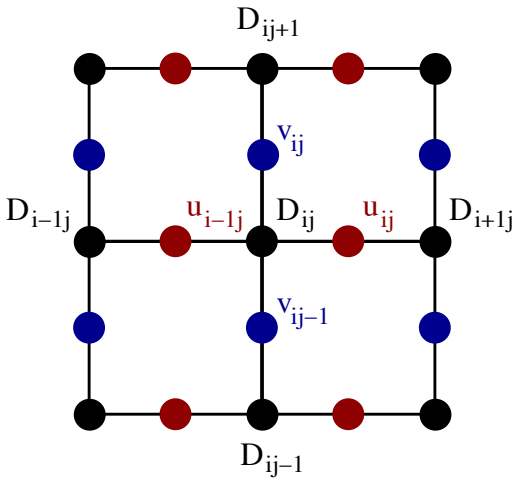

Figure 1: A graphical sketch of the horizontal **D**-grid staggering of the velocity components u and v as well as the spatial 'location' of divergence that is used by the divergence damping operators.

For even higher-order divergence damping ($n = 6, 8, ..$) the ∇^2-operator could be applied iteratively to discretize the ∇^n-operator (not explored in this paper). Note that the higher the order of the divergence damping the wider the stencil needed for its discretization.

The spatial discretization of the divergence damping terms in the momentum equations using centered differences then becomes

$$\frac{\partial u_{ij}}{\partial t} = \cdots + \frac{1}{a\cos\theta_{j-1/2}}\frac{1}{\Delta\lambda}\left[(\gamma_n\nabla^{n-2}D)_{i+1j} - (\gamma_n\nabla^{n-2}D)_{ij}\right], \tag{11}$$

$$\frac{\partial v_{ij}}{\partial t} = \cdots + \frac{1}{a}\frac{1}{\Delta\theta}\left[(\gamma_n\nabla^{n-2}D)_{ij+1} - (\gamma_n\nabla^{n-2}D)_{ij}\right]. \tag{12}$$

respectively, where γ_n is evaluated at the respective 'divergence'-points (edge-points). The explicit formulas for γ_n are given in the next section.

2.3. Divergence damping coefficients

2.3.1. Second-order divergence damping γ_2

In the original formulation of CAM-FV second-order divergence damping ($n = 2$) is used with damping coefficient

$$\gamma_2 = (\gamma_2)_k = \tau_k \frac{\mu_2\,(a^2\Delta\lambda\Delta\theta)}{\Delta t}, \tag{13}$$

where k is the vertical level index, Δt is the time-step, $\mu_2 = 1/128$ and the weight function τ_k is 1 throughout the atmosphere except in the top model levels (sponge layer) where it monotonically increases to approximately 4 at the top of the atmosphere (see Fig. 2)

$$\tau_k = \mu_2\ \max\left\{1, 8\left[1 + \tanh\left(\log\left(\frac{p_{top}}{p_k^{ref}}\right)\right)\right]\right\}, \tag{14}$$

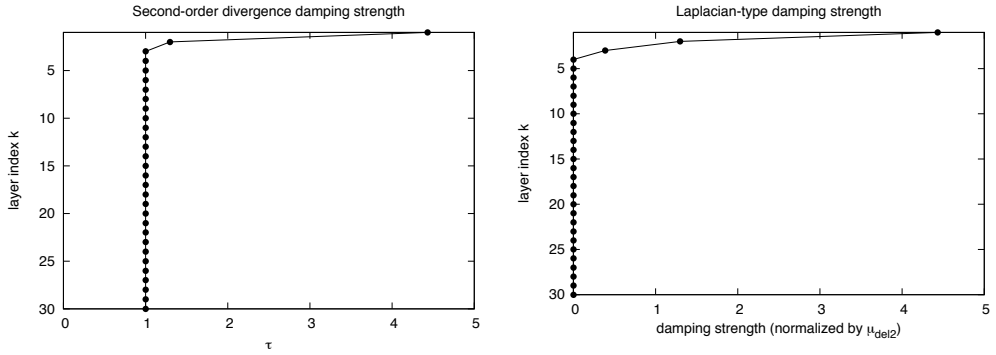

Figure 2: (left) Second-order divergence damping strength function τ_k as a function of vertical level index k in CAM5. The level index is 1 at the model top and increases monotonically towards the surface. (right) Strength of the 'Laplacian' damping γ_{del2} (in units of μ_{del2}) as a function of level index.

where p_{top} is the pressure at the top of the model (p_{top} is typically 2 hPa) and p_k^{ref} is the reference pressure at the center of the cell

$$p_{k+1/2}^{ref} = \frac{1}{2}\left[A_k + A_{k+1} + 10^5\ (B_k + B_{k+1})\right]. \tag{15}$$

Here A_k and B_k are the coefficients for the hybrid vertical coordinate. Linear theory predicts that the second-order divergence damping is stable when μ_2 is chosen such that

$$\mu_2\ \max\left(\alpha, \frac{1}{\alpha}\right) \leq \frac{1}{4}, \tag{16}$$

(Whitehead et al., 2010) where α is the grid aspect ratio $\alpha = \Delta\lambda/\Delta\theta$.

2.3.2. Fourth-order divergence damping γ_4

By setting $n = 4$ fourth-order divergence damping is invoked where, in CAM-FV, the coefficient is set to

$$\gamma_4 = \mu_4\ \left(a^2 \cos(\theta)\Delta\lambda\Delta\theta\right)^2 / \Delta t, \tag{17}$$

where $\mu_4 = 1/100$ throughout the atmosphere. Since divergence damping is added explicitly to the equations of motion it may lead to instability if the time-step is too large or the damping coefficients (γ_2 or γ_4) are too large. To stabilize the fourth-order divergence damping a latitudinal dependence ($\cos(\theta)$) has been 'added' to (17) and the winds used to compute the divergence damping tendencies are filtered using the same FFT (Fast Fourier Transform) filtering along latitudes that is applied to stabilize the gravity waves (Neale et al., 2010a).

A one-dimensional linear stability analysis of divergence damping will show that the damping factor as a function of wavelength is a monotonically increasing function for which higher wavenumbers (smaller wavelengths) are damped more. Generally, fourth-order damping is more scale selective than second-order damping in that shorter wavelengths are damped more and longer wavelengths are damped less. For a fuller discussion on the linear dispersion properties

of both second and fourth-order divergence damping operators when implemented on the sphere using the regular latitude-longitude grid see Whitehead et al. (2010).

For stability and accuracy it is recommended that μ_4 be chosen such that

$$\mu_4 \max\left(\alpha, \frac{1}{\alpha}\right) \leq \frac{6}{625}, \tag{18}$$

(Whitehead et al., 2010).

2.4. 'Laplacian' top-of-atmosphere damping

To slow down the potentially excessive polar night jets in high-resolution configurations of CAM-FV and to enhance the top-of-atmosphere sponge layer, 'Laplacian'-type damping of the wind components has been added as an option in CAM5. That is, the following terms are added to the momentum equations

$$\frac{\partial u}{\partial t} = \cdots + \gamma_{del2}\nabla^2 u, \tag{19}$$

$$\frac{\partial v}{\partial t} = \cdots + \gamma_{del2}\nabla^2 v. \tag{20}$$

The damping coefficient γ_{del2} is zero throughout the atmosphere except in the top layers (sponge layer) where it increases monotonically and smoothly from zero to approximately four times a user-specified damping coefficient μ_{del2} at the top of the atmosphere (the user-specified damping coefficient is typically $\mu_{del2} = 3.0 \times 10^5$ m^2/s). That is,

$$\gamma_{del2} = (\gamma_{del2})_k = \begin{cases} 0, & \tau_k < 0.3 \\ \tau_k \mu_{del2} & \text{else.} \end{cases} \tag{21}$$

The scalar Laplacian operator applied in (19) and (20) is not equivalent to the full vector Laplacian (see, e.g., Jablonowski and Williamson 2010). Hence we refer to this damping in the top-of-atmosphere sponge layer as 'Laplacian' in quotes as it differs from the true vector Laplacian. Other mechanisms in CAM-FV that provide sponge-layer features are the reduction of the horizontal advection operator to first-order in the top model layers as well as first-order remapping in the vertical near the domain top (and bottom).

3. Results

The effects of the new damping operators on CAM-FV simulations are discussed in four different sections below. First, the effects of divergence damping operators on the TKE spectra are discussed. Next the level of noise in the divergence field from instantaneous velocity fields in a 'typical' CAM-FV simulation are shown and discussed. In the third section the beneficial effects (in terms of noise levels) of using fourth-order divergence damping in CAM-FV DART is discussed. Finally we show the effects of the top-of-atmosphere 'Laplacian' damping operator on climate simulations for some key dynamics variables.

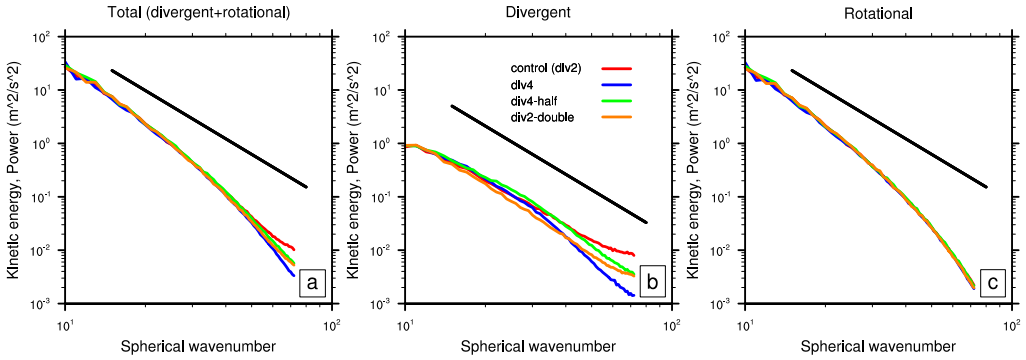

Figure 3: (a) Total kinetic energy (TKE) spectrum as a function of spherical wavenumber h using second-order (red line using $\mu_2 = 1/128$; orange line using $\mu = 2/128$) and fourth-order divergence damping (blue line using $\mu_4 = 1/100$; green line using $\mu_4 = 1/200$). The spectra are computed from daily instantaneous wind data averaged over 30 days using CAM5 at $1.9^\circ \times 2.5^\circ$ resolution. In (b) and (c) the TKE is broken into divergent and rotational components, respectively. The solid black line is the h^{-3} reference slope (Nastrom and Gage, 1985).

3.1. Total kinetic energy (TKE) spectra

Figure 3 shows the TKE spectrum averaged over a 30-day period for daily instantaneous winds around 200 hPa (model level k=13) as a function of spherical wavenumber h for different CAM-FV configurations at $1.9^\circ \times 2.5^\circ$ resolution using the CAM5 physical parameterization package. The TKE spectrum is broken into divergent and rotational components in Fig. 3(b) and Fig. 3(c), respectively. As shown analytically in (7) and (8), the divergence damping operators only affect the divergent part of the wind field and do not affect the rotational part. The original CAM-FV configuration uses second-order divergence damping ($n = 2$) with $\mu_2 = 1/128$ and we note that TKE accumulates at the shortest wavelengths (tail of the TKE in Fig. 3(b) is concave up). This spurious accumulation of TKE near the grid scale can be alleviated by doubling the second-order divergence damping coefficient ($\mu_2 = 2/128$) at the expense of unnecessarily damping longer wavelengths (orange curve in Fig. 3(b) is below all other curves for spherical wavenumbers larger than approximately $h = 15$). A more scale-selective damping can be achieved by using fourth-order divergence damping with $\mu_4 = 1/100$ (blue curve in Fig. 3(b)). The tail of divergent part of the TKE is, roughly speaking, controlled by the damping coefficients such as illustrated for the fourth-order divergence damping where a halving of the damping coefficient $\mu_4 = 1/200$ 'pulls-up' the high wavenumber end of the curve.

The TKE results together with the visual noise level in the divergence field presented in the next section, seem to indicate that $\mu_4 = 1/100$ is a good compromise between alleviating noise and providing a TKE spectrum without spurious accumulation of energy near the grid scale. All of the configurations seem to exhibit a TKE slope that is steeper than h^{-3} and higher horizontal resolutions are needed to obtain a h^{-3} slope in the $h \in [20, 50]$ range (see, e.g., Jablonowski and Williamson 2010).

3.2. Instantaneous divergence field in CAM-FV

To demonstrate the effect on divergence of higher-order divergence damping in CAM-FV, we use the same setup as in the previous section (CAM5 physical parameterization suite and

$1.9^\circ \times 2.5^\circ$ resolution). Fig. 4 shows the instantaneous divergence D_{ij} at model level 13 (approximately 200 hPa) computed using the discretization of divergence used in CAM-FV [3] given in (9), for different divergence damping configurations. First we note that the original second-order divergence damping configuration does not eliminate grid-scale noise in the divergence field. The noise tends to be aligned with latitudes and for the particular day shown in Fig. 4 the noise is particularly apparent off the west coast of Africa and over the Saudi-Arabian peninsula (white color circles on Fig. 4a). Doubling the second-order divergence damping coefficient alleviates the noise but does not remove it (see Fig. 4b - off the coast of west Africa). As observed in the TKE analysis above, a doubling of μ_2 unnecessarily damps longer wavelength. Fourth-order divergence damping configurations with $\mu_4 = 1/100$ (Fig. 4c) and $\mu_4 = 1/200$ (Fig. 4d), respectively, alleviates the noise in the divergence field for the particular case shown in Fig. 4.

It is hard to be certain that the noise in the 4 day forecast was eliminated due to enhanced damping rather than the chaotic evolution of the modified model trajectories because the noise in the divergence field appears sporadic in space and time. However, there seem to be high correlations between zonal wind speed and noise levels as illustrated in Fig. 5. The noise in the divergence field is predominantly aligned with latitudes; hence the difference between the 'raw' divergence field and the divergence field filtered with a 1-2-1 filter along longitudes emphasizes regions with noise. Fig. 5(a-d) show the monthly average of RMS (root mean square) for this difference field and Fig. 5(e) shows the monthly averaged zonal wind component. In particular, high zonal wind-speed regions over the Pacific Ocean and off the East coast of USA are prone to noise in the divergence field. Noise levels are significantly reduced with fourth-order divergence damping using $\mu_4 = 1/100$; however, since the fourth-order divergence damping strength decreases with latitude the polar regions are more noisy compared to the run with second-order divergence damping.

3.3. Divergence damping in CAM-FV DART

The noise problems in the CAM-FV using second-order divergence damping were initially detected by using CAM-FV with the DART ensemble Kalman filter data assimilation system in a numerical weather prediction application. The DART ensemble Kalman filter (Anderson, 2001) combines an ensemble of 80 6-hour CAM4 (Neale et al., 2010b) forecasts with observations to produce an ensemble analysis every 6 hours. The observations used were those in the NCAR-NCEP reanalysis including winds and temperatures from radiosondes and aircraft, and cloud motion vector winds, totaling roughly half a million observations per day. The assimilation used advanced ensemble techniques including spatially and temporally varying adaptive inflation (Anderson, 2009), spatial localization of observations (Houtekamer and Mitchell, 2001) and quality control of observations by comparing with the prior ensemble.

In densely observed regions, the data assimilation process can reduce the noise generated by the model forecasts. However, in more sparsely observed regions, noise in the observations can project onto model states so that noise in the model forecasts is amplified. Replacing second-order divergence ($\mu_2 = 1/128$) damping with fourth-order divergence ($\mu_4 = 1/100$) damping significantly reduced the level of the noise in the assimilated states (see Fig. 6).

Data assimilation is a good tool for detecting this kind of noise in a climate model because observations constrain the ensemble of states to be close to particular real atmospheric states.

[3] note that if computing divergence using centered finite-difference based on wind components averaged to the cell centers, the grid-sale noise is averaged out through the centered finite-difference approximations and averaging

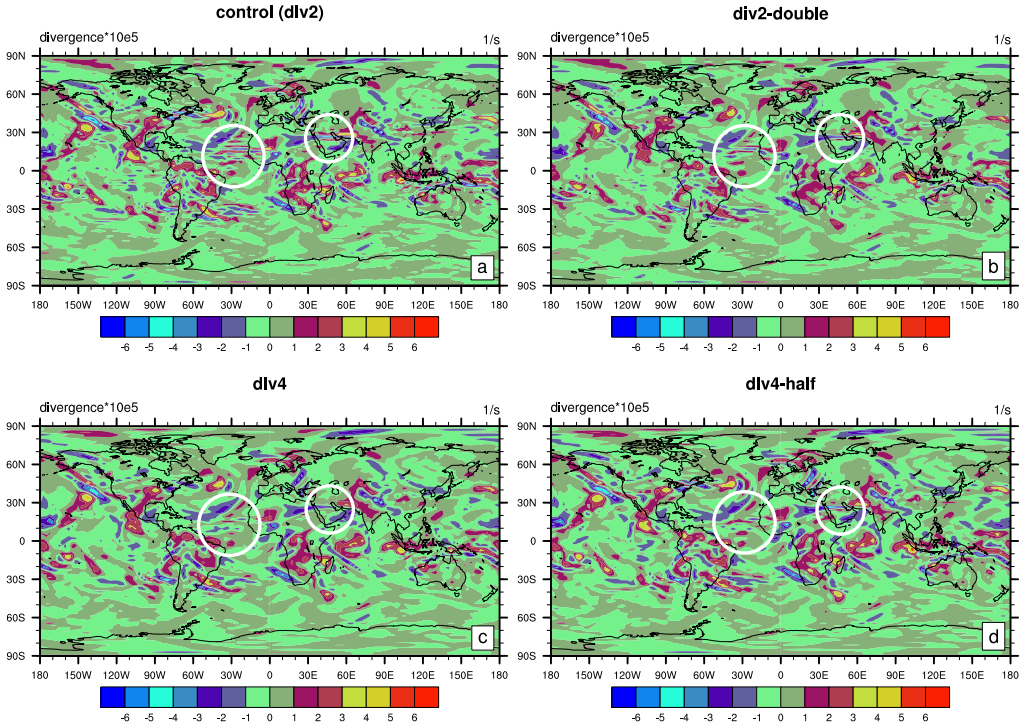

Figure 4: Contour plots of instantaneous divergence in units of $10^5/s$ at model level k=13 (approximately 200 hPa) at day 4 starting from '31 Dec 1998'-initial conditions using (a) the 'original' second-order divergence damping ($\mu_2 = 1/128$), (b) second-order divergence damping with a doubling of damping coefficient ($\mu_2 = 2/128$), (c) fourth-order divergence damping with $\mu_4 = 1/100$ and (d) fourth-order divergence damping with $\mu_4 = 1/200$. CAM5 physics was used and the resolution was 1.9°×2.5°. In (a) note the noise west of Africa and over the Saudi-Arabian peninsula (indicated by white color circles).

One can then readily evaluate whether noise is reduced for a particular synoptic situation without being concerned by the chaotic nature of longer model forecasts.

3.4. Laplacian damping in CAM-FV

A series of climate simulations with fixed sea surface temperatures have been performed using the CAM4 physical parameterization suite at increasing horizontal resolutions using the 'default' parameter settings of the $1.9° \times 2.5°$ setup. The stratospheric polar night jet spuriously increases as a function of horizontal resolution (see first row in Fig. 7). By introducing the 'Laplacian' sponge layer the stratospheric polar night jet is significantly reduced in magnitude. At approximately 2° horizontal resolution the original CAM4 does not exhibit an excessive polar night jet and the 'Laplacian' sponge layer damping slows down the jet too much. However, at approximately 1/2° horizontal resolution the winds in the runs with the 'Laplacian' sponge layer are improved significantly with respect to NCAR-NCEP reanalysis data. This is also reflected in the temperature fields (not shown).

In CAM-FV at approximately $1/4^\circ$ ($0.23^\circ \times 0.31^\circ$) horizontal resolution the need for higher-order divergence damping (for stability) and enhanced sponge layer is even greater. Due to the computational expenses of running CAM4 at this 'ultra-high' resolution, the runs are relatively short (on the order of years) and therefore the results are indicative rather than conclusive. The sponge layer damping is not only influencing the stratospheric jets but also the sea-level pressure as shown in Fig. 8 (second row). The value of μ_{del2} used for the lower-resolution runs described above does not seem to damp the polar night stratospheric jets enough (second-column in Fig. 8) whereas increasing it to $\mu_{del2} = 4 \times 10^5$ m^2/s slows down the jets and improves the excessive low near Iceland in the sea-level pressure field. Another factor that may influence the sea-level pressure is the gravity wave parameterization, for example, by altering the effective scale at which momentum of parameterized gravity waves are deposited (k_{wv}).

The sea-level pressure pattern is also sensitive to the strength of parameterized mountain wave drag in the model. By specifying an 8x higher wavenumber k_{wv} for orographic waves at $0.23^\circ \times 0.31^\circ$ horizontal resolution, an improved sea-level pressure pattern is obtained, comparable to that obtained from increasing μ_{del2} (third column in Fig. 8). The total mountain wave momentum flux at the surface should increase roughly as k_{wv}, without significant changes to the deposition level in the vertical. Thus mountain wave drag in the upper troposphere/lower stratosphere should also increase as k_{wv}. While strengthening this presumably physical drag source may allow reductions in numerical filtering it is unlikely that it will entirely eliminate the need for it. This is an area of on-going research.

4. Conclusions

This paper documents the implementation of new damping/filtering operators in NCAR's CAM-FV model. The motivation for replacing the original second-order divergence damping in CAM-FV with fourth-order divergence damping was the observation of grid-scale noise in CAM-FV simulations. These noise levels could lead to model failure, in particular, at high spatial resolutions. It is demonstrated through a total kinetic energy analysis, examination of instantaneous divergence fields in CAM-FV and by looking at the meridional wind component in ensemble members during data-assimilation (CAM-FV DART), that the fourth-order divergence damping alleviates the noise problems. Moreover it leads to a more robust model.

In addition to the divergence damping operator, the sponge layer at the top of the atmosphere was modified with a 'Laplacian'-type damping of the velocity components. The motivation for such a sponge-layer damping was the excessive polar night jets that develop at high spatial resolutions when running the original CAM-FV. The 'Laplacian'-type damping of the velocity components successfully slowed down the excessive polar night jets at high horizontal resolutions and produced more realistic simulations in terms of zonal wind speed, sea-surface pressure and temperature distribution.

Acknowledgements

This work performed under the auspices of the U.S. Department of Energy by Lawrence Livermore National Laboratory (LLNL) under Contract DE-AC52-07NA27344. Computer time on Livermore Computing's Atlas machine was provided under LLNL's Multiprogrammatic & Institutional Computing Initiative. Computing for DART experiments was provided by NSF's Climate Simulation Laboratory.

References

Anderson, J., Hoar, T., Raeder, K., Liu, H., Collins, N., Torn, R., Avellano, A., 2009. The data assimilation research testbed: A community facility. Bull. Amer. Meteor. Soc. 90, 1283–1296.

Anderson, J. L., 2001. An ensemble adjustment Kalman filter for data assimilation. Mon. Wea. Rev. 129, 2884–2903.

Anderson, J. L., 2009. Spatially and temporally varying adaptive covariance inflation for ensemble filters. Tellus A 61, 72–83.

Bates, J. R., Moorthi, S., Higgins, R. W., 1993. Global multilevel atmospheric model using a vector semi-Lagrangian finite-difference scheme. Part I: Adiabatic formulation. Mon. Wea. Rev. 121 (1), 244–263.

Haltiner, G. J., Williams, R. T., 1980. Numerical Prediction and Dynamic Meteorology. John Wiley & Sons, 477 pp.

Houtekamer, P. L., Mitchell, H. L., 2001. A sequential ensemble Kalman filter for atmospheric data assimilation. Mon. Wea. Rev. 129, 123–137.

Jablonowski, C., Williamson, D. L., 2010. The pros and cons of diffusion, filters and fixers in atmospheric general circulation models., in: P.H. Lauritzen, R.D. Nair, C. Jablonowski, M. Taylor (Eds.), Numerical techniques for global atmospheric models. Lecture Notes in Computational Science and Engineering, Springer, 2010, in press.

Lauritzen, P. H., 2007. A stability analysis of finite-volume advection schemes permitting long time steps. Mon. Wea. Rev. 135, 2658–2673.

Lin, S.-J., 2004. A 'vertically Lagrangian' finite-volume dynamical core for global models. Mon. Wea. Rev. 132, 2293–2307.

Lin, S. J., Rood, R. B., 1996. Multidimensional flux-form semi-Lagrangian transport schemes. Mon. Wea. Rev. 124, 2046–2070.

Lin, S.-J., Rood, R. B., 1997. An explicit flux-form semi-Lagrangian shallow-water model on the sphere. Q.J.R.Meteorol.Soc. 123, 2477–2498.

Nastrom, G. D., Gage, K. S., 1985. A climatology of atmospheric wavenumber spectra of wind and temperature observed by commercial aircraft. J. Atmos. Sci. 42, 950–960.

Neale, R. B., Chen, C.-C., Gettelman, A., Lauritzen, P. H., Park, S., Williamson, D. L., Conley, A. J., Garcia, R., Kinnison, D., Lamarque, J.-F., Marsh, D., Mills, M., Smith, A. K., Tilmes, S., Vitt, F., Cameron-Smith, P., Collins, W. D., Iacono, M. J., Easter, R. C., Ghan, S. J., Liu, X., Rasch, P. J., Taylor, M. A., 2010a. Description of the NCAR Community Atmosphere Model (CAM 5.0). NCAR Technical Note, National Center of Atmospheric Research.

Neale, R. B., Chen, C.-C., Gettelman, A., Lauritzen, P. H., Park, S., Williamson, D. L., Conley, A. J., Garcia, R., Kinnison, D., Lamarque, J.-F., Marsh, D., Mills, M., Smith, A. K., Tilmes, S., Vitt, F., Cameron-Smith, P., Collins, W. D., Iacono, M. J., Easter, R. C., Ghan, S. J., Liu, X., Rasch, P. J., Taylor, M. A., 2010b. Description of the NCAR Community Atmosphere Model (CAM 4.0). NCAR Technical Note, National Center of Atmospheric Research.

Skamarock, W. C., 2008. A linear analysis of the NCAR CCSM finite-volume dynamical core. Mon. Wea. Rev. 136, 2112–2119.

Whitehead, J., Jablonowski, C., Rood, R. B., Lauritzen, P. H., 2010. A stability analysis of divergence damping on a latitude-longitude grid. Mon. Wea. Rev.Revising.

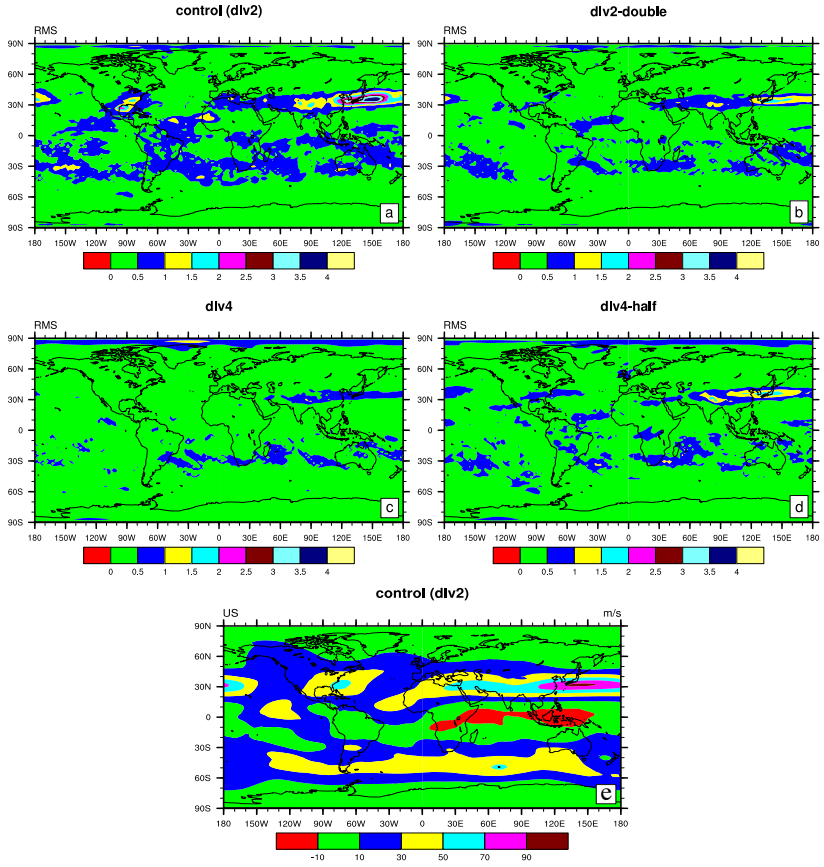

Figure 5: (a-d) Same as Fig. 4 but for the monthly average (January 10 to February 10, 1999) of the RMS value of the difference between divergence and divergence filtered along longitudes with a 1-2-1 filter. High values of RMS generally indicate regions with strong noise at the grid scale in the divergence field. The lower plot (e) is the staggered zonal wind averaged over the same period of time.

(a) Second–order divergence damping

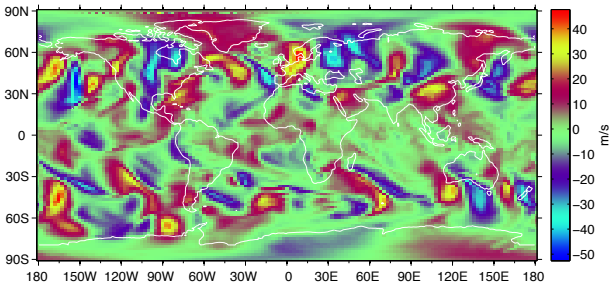

(b) Fourth–order divergence damping

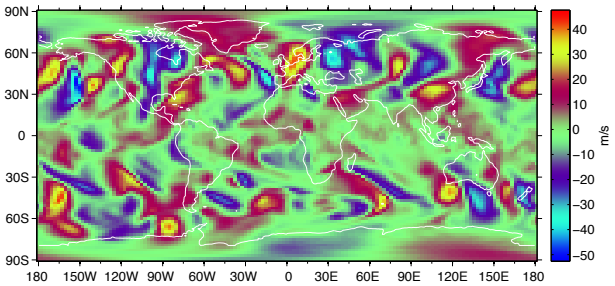

(c) Difference

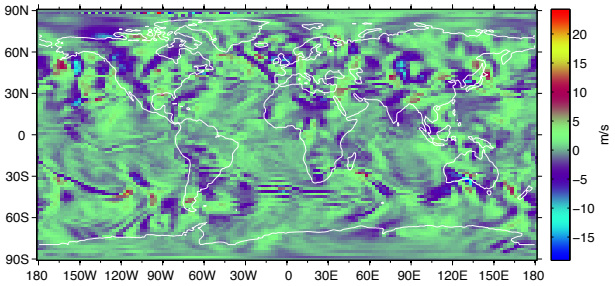

Figure 6: CAM-DART results. (a) The 6-hour forecast, using the second-order divergence damping ($\mu_2 = 1/128$), of the instantaneous, staggered, meridional wind v at approximately 266 hPa. The initial conditions are a single ensemble member analysis taken from a $1.9^\circ \times 2.5^\circ$ CAM-FV, DART/CAM4.0 assimilation at 12/5/2000 00Z. (b) The same as (a), but using the fourth order divergence damping ($\mu_4 = 1/100$). (c) The second-order damping forecast minus the fourth-order forecast highlights the reduction in grid-scale noise. The data is plotted on the regular latitude-longitude grid without interpolation. Hence diagonal patterns/edges may look noisy even though they are not.

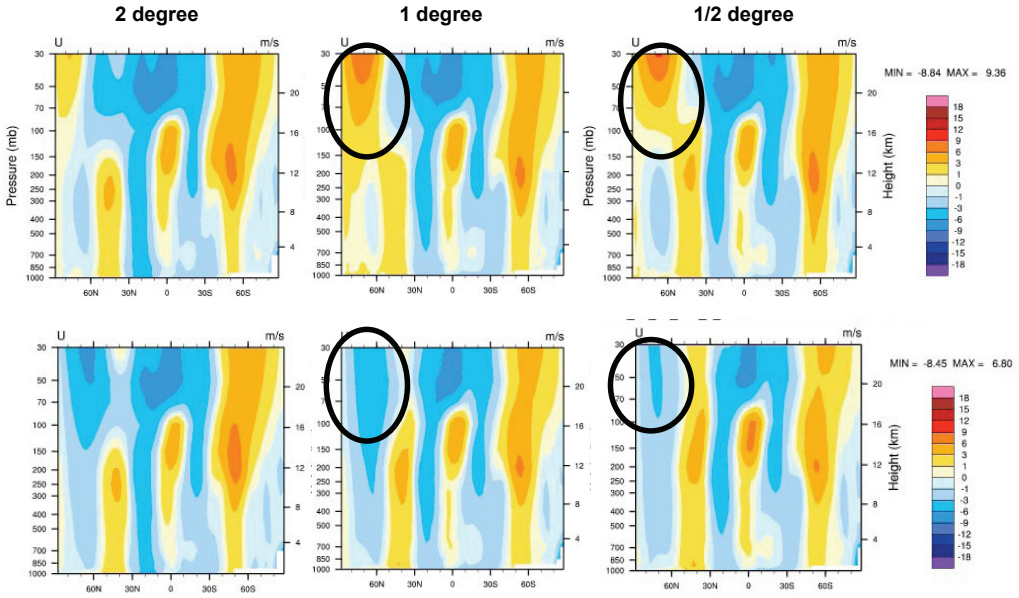

Figure 7: Differences in December/January/February averaged zonal wind speed between a CAM4 10-year mean (years 2-11) and the NCAR-NCEP reanalysis climatology. First row is for 'default' CAM-FV using second-order divergence damping ($\mu_2 = 1/128$). Second row is with second-order damping replaced with fourth-order divergence damping ($\mu_4 = 1/100$) and 'Laplacian' damping/sponge near the model top ($\mu_{del2} = 3 \times 10^5$ m^2/s). Left, middle and right columns are for the approximately 2°, 1° and $1/2^\circ$ horizontal resolutions, respectively. The circles indicate the approximate location of the Northern hemisphere winter stratospheric jet.

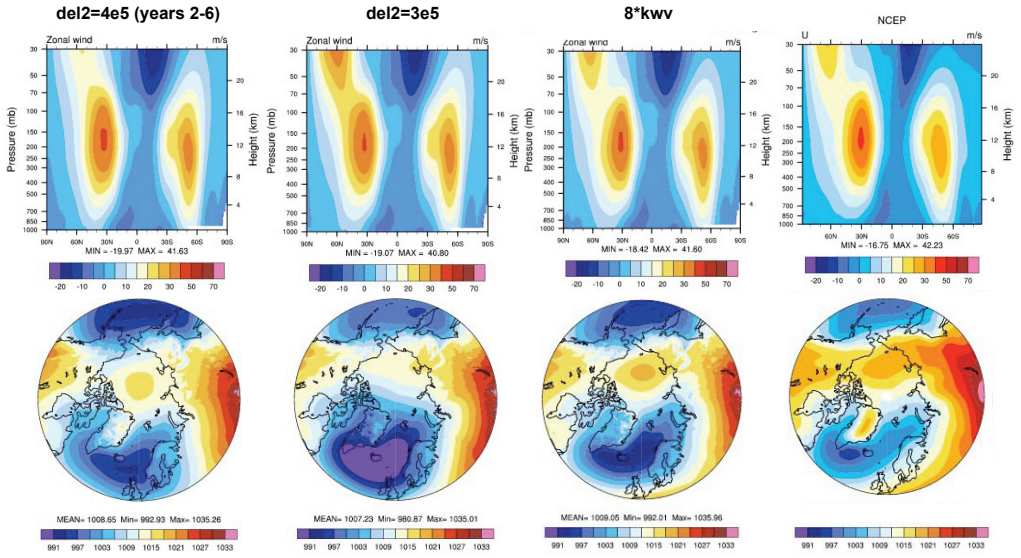

Figure 8: Results for CAM4 at approximately 1/4° (0.23°×0.31°) horizontal resolution. First and second rows are zonal wind speed and sea-level pressure, respectively. Fields in the first column are 5 year averages during Northern Hemisphere winter (December, January, February) whereas fields displayed in the second and third columns are 2 year averages using 'spun-up' initial conditions from the run in the first column. First, second and third columns are based on runs with a 'Laplacian' sponge layer with damping coefficient $\mu_{del2} = 4\times10^5$ m^2/s, $\mu_{del2} = 3\times10^5$ m^2/s, and $\mu_{del2} = 3\times10^5$ m^2/s, respectively. In the third column also k_{wv}, a gravity wave parameterization parameter, was altered by multiplying its 'default' value eight-fold. The fourth column is the climatological mean from the NCAR-NCEP reanalysis for the corresponding fields.